Atmospheric temperature variability in the Arctic as revealed in a TOVS data record

Siri Jodha Singh Khalsa
Applied Research Corporation, 8201 Corporate Drive, Suite 1120, Landover, MD 20785, USA
Jeffrey R. Key
Cooperative Institute for Research in Environmental Sciences, Campus Box 449, University of Colorado, Boulder, CO 80309-0449, USA

Received July 1994

ABSTRACT. The Earth's high-latitude regions are of critical importance in many climate-change scenarios, but a time-continuous, spatially complete, and well-calibrated record of tropospheric temperatures is needed in order to assess past and future climate changes. Studies of recently compiled upper-air data sets show no evidence of CO_2-induced warming, but the spatial pattern of tropospheric temperature variability in the Arctic has not been thoroughly examined. This study analyzes a 108-month segment of the data record from the TIROS Operational Vertical Sounder (TOVS) aboard NOAA polar-orbiting satellites to examine both the spatial and temporal variability of atmospheric temperature in the Arctic.

Temperature retrievals based on clear-column radiances archived at NOAA/NESDIS were done using algorithms tuned to Arctic conditions. The retrieved temperatures compared well with Arctic rawinsonde data, and include low-level inversions that are often problematic for satellite retrievals. The amplitude of the seasonal cycle in 500 mbar temperatures from the TOVS, NMC, and rawinsonde data generally agreed, whereas the phase comparisons produced mixed results. Principal component analyses of the TOVS and NMC temperatures revealed both monopole and dipole spatial patterns in the component loadings. Spatial patterns of the correlation between the upper-air data and the TOVS retrievals were similar to the principal component loading patterns. Whereas no significant trends were found in the station data for the same period as the TOVS record, a significant negative trend could be seen in the first principal component scores of the TOVS retrievals.

Contents

Introduction

Concern over possible climatic impacts of increased CO_2 and other greenhouse gases has prompted increasing attention to be focused on the Arctic. Many consider this region to be an especially sensitive indicator of climate change (for example, Wetherald and Manabe 1988), a view that is supported by modeling studies. To date, observational studies of Arctic temperatures have relied on a relatively sparse network of surface and upper-air stations at coastal and inland locations, leaving vast areas of the Arctic Basin unsampled. Recent examinations of the observational record of Arctic temperatures are, however, contradictory. Hansen and Lebedeff (1987) found that Arctic air temperatures have increased since 1880; Kahl and others (1993a; 1993b) did not find evidence of greenhouse-induced warming in the Arctic troposphere during the period 1958–1986.

Theoretical studies indicate that the expected climatic warming in the Arctic will be strongest at the surface but will extend throughout the lower troposphere with increasing intensity toward the pole. Manabe and others (1992) reported modeled surface temperature increases due to greenhouse warming on the order of 6° C in the Arctic, with mid-tropospheric increases on the order of 2.5° C. Interpretation of the surface record in Arctic climate-change studies is complicated by the high frequency of strong surface-based inversions that can cause a decoupling of the surface from the dynamics of the mid and upper troposphere. However, surface temperatures remain radiatively coupled to tropospheric conditions, principally through cloud cover. In any case, Arctic climate monitoring should include an examination of temperatures at all levels of the troposphere and, additionally, the stratosphere, where cooling is expected.

This paper assesses the suitability of data from the polar-orbiting TIROS Operational Vertical Sounder (TOVS) for providing a detailed, spatially complete analysis of temperature variability in the northern hemisphere north of 60° latitude. Comparisons of TOVS temperature retrievals with rawinsonde data are first done in an attempt to assess their accuracy. Spatial patterns are then examined through the use of principal components analysis (PCA) of TOVS-derived temperatures and National Meteorological Center (NMC) fields. Lastly, trends in the principal component scores for both data sets during the period of record are presented. Analyses of spatial patterns and trends are restricted to the middle troposphere, at approximately the 500 mbar level. Monthly mean temperatures for the period 1983–1991 are examined.

Data

The primary data set in this analysis consisted of temperature profiles retrieved from TOVS radiances. Temperatures from two other data sets were used for comparison: *in situ* rawinsonde data and NMC analyses.

TOVS retrievals

The TOVS system is comprised of three sensors: the high-resolution infrared radiation sounder (HIRS), the microwave sounding unit (MSU), and the stratospheric sounding unit (SSU). Only the HIRS and MSU sensors were used in this study. HIRS measures radiation in 19 infrared

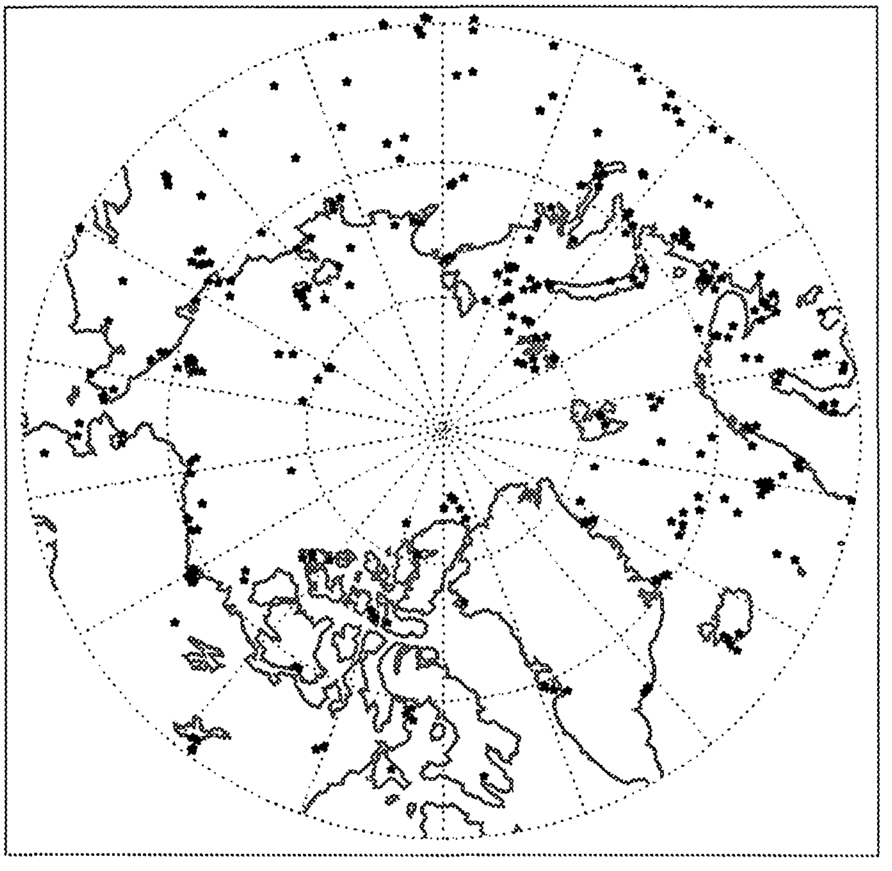

Fig. 1. Locations of the Arctic profiles incorporated into the TIGR database.

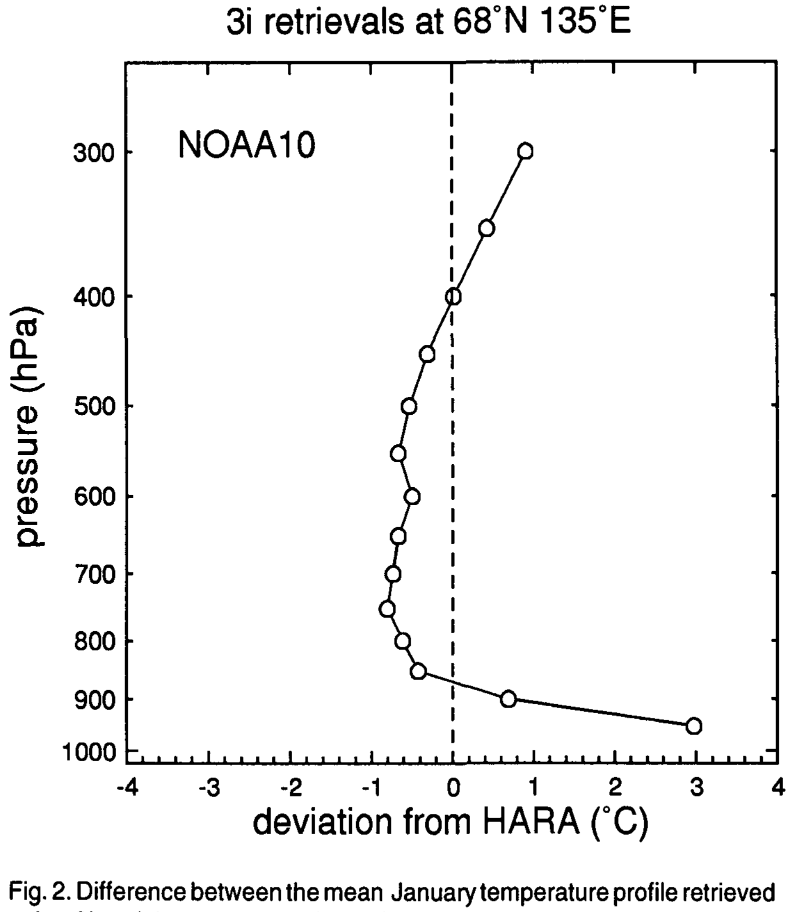

Fig. 2. Difference between the mean January temperature profile retrieved using 3I and the nearest rawinsonde data.

(IR) bands from 3.7 to 15 μm and one shortwave band at 0.7 μm. The MSU measures radiation at four frequencies between 50 and 58 GHz. Both instruments scan from nadir to 58° on either side of nadir with a resulting swath width of 2200 km. HIRS and MSU have nadir resolutions of 17 and 110 km, respectively.

The National Environmental Satellite and Data Information Service (NESDIS) of the US National Oceanographic and Atmospheric Administration (NOAA) has been producing an operational sounding product for assimilation into numerical weather prediction models since 1979. These temperature retrievals were not used because the NESDIS algorithms have changed over the years, the algorithms do not perform well in Arctic conditions, and their statistical retrieval methods are strongly biased towards climatology. Instead, an intermediate product of their retrieval process was used: the clear-column radiances (McMillin and Nappi 1986).

An important first step in interpreting infrared radiance data from satellites is determining whether the scene being observed contains clouds. NESDIS first tests whether there are any completely clear scenes. If not, the radiances from a group of partially cloud-filled scenes is adjusted to give what the radiances would be in the absence of clouds. If this also fails, the scenes are declared cloudy, and retrievals are done using only those channels whose weighting functions are high enough in the atmosphere to be unaffected by clouds. Radiances from these type of soundings were not used in this study.

Since the retrievals were performed in areas that were clear or partly cloudy, the results could be biased towards colder surface conditions. This is because the sampling excluded regions under persistent cloud cover, which tend to have higher surface temperatures, particularly in winter. In the monthly averages, we assumed enough partly cloudy regions were sampled to minimize this effect.

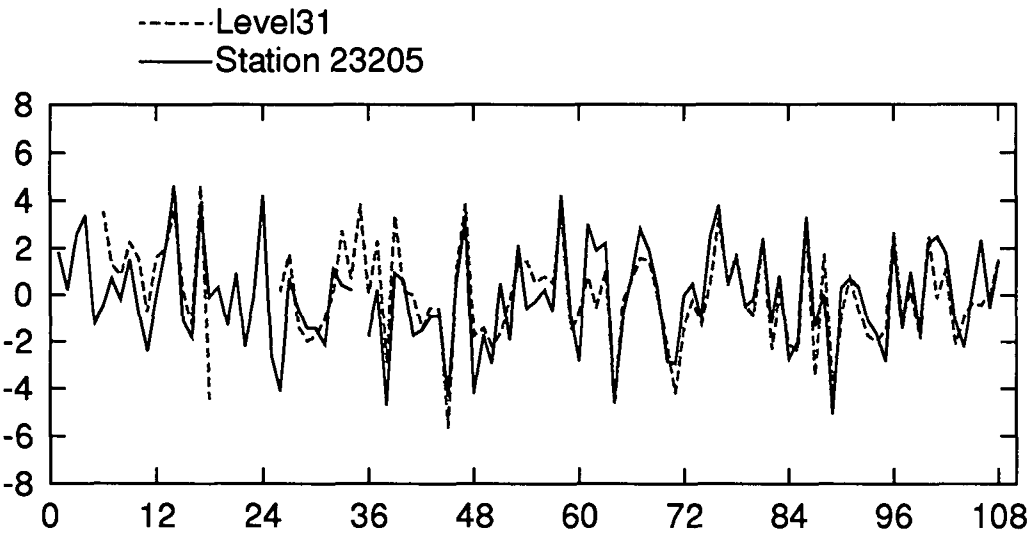

Fig. 3. Time series of monthly mean temperature anomalies near the 500 mbar level from TOVS and an upper-air station, from June 1983 through December 1991.

Temperature profiles were retrieved from the clear-column radiances using the Improvèd Initialization Inversion method (3I; Chedin and others 1985). The 3I method combines both physical and statistical techniques to obtain estimates of geophysical quantities from the HIRS and MSU radiances. One of the most important steps in the retrieval of a temperature profile, both in 3I and in other TOVS processing systems, is the first guess profile. The 3I system incorporates the TOVS Initial Guess Retrieval (TIGR) database of representative atmospheric profiles, based on a global set of more than 150,000 radiosonde measurements. A forward radiative transfer model is used to compute channel radiances and brightness temperatures, transmittances, and covariances between temperatures and radiances. This is done for each profile at 10 viewing angles, 19 surface pressures, and two surface emissivities. Temperature profiles are classified into one of five air mass types: one tropical, two mid-latitude, and two polar, according to their statistical characteristics.

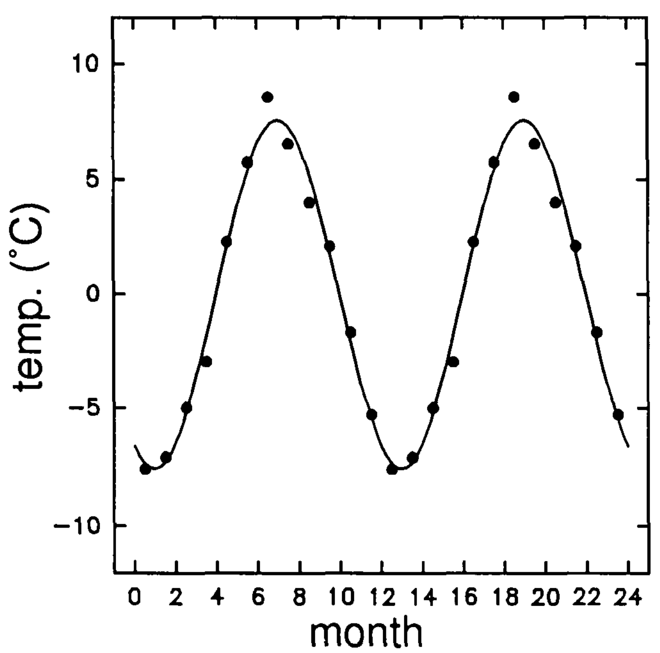

Fig. 4. Example of fitting the seasonal cycle to temperature data from one Arctic station.

Version 2 of TIGR contains 1761 atmospheric situations, of which 441 come from soundings north of 60°N. Figure 1 shows the locations of these soundings. While most were from coastal stations, the central ice pack was also represented by soundings collected at Soviet drifting (ice) stations (Serreze and others 1992). Comparisons of TIGR profiles with rawinsonde data have shown it to contain a reasonably complete representation of Arctic conditions (Key and others 1993).

The 3I processing was normally done in four distinct steps, with the temperature retrievals occurring in the fourth step. The first three steps of the 3I package were not necessary when starting from the clear-column radiances supplied from NESDIS. However, several operations done in the first three steps of 3I produced results that were needed in the fourth, so some modification of the source code was necessary. Additionally, the polar-specific modifications of 3I described in Francis (1994) were incorporated. These have also been integrated into the latest official version of 3I. The modifications include detection of sea ice, an improved estimate of sea-ice emissivity, and polar-night cloud detection.

At present, retrievals are only performed on data from the NOAA-8, NOAA-9, NOAA-10, and NOAA-11 satellites, those for which the radiance bias corrections factors are included in the 3I code. This covers the period June 1983 through December 1991, with one gap of eight months when none of the above satellites was operational. A comparison of monthly mean 500 mbar temperatures for the different satellites was done. The amplitude of the seasonal cycle was about 20°. In the regions of overlap, the NOAA-10/NOAA-11 overlap being the longest, consistent biases

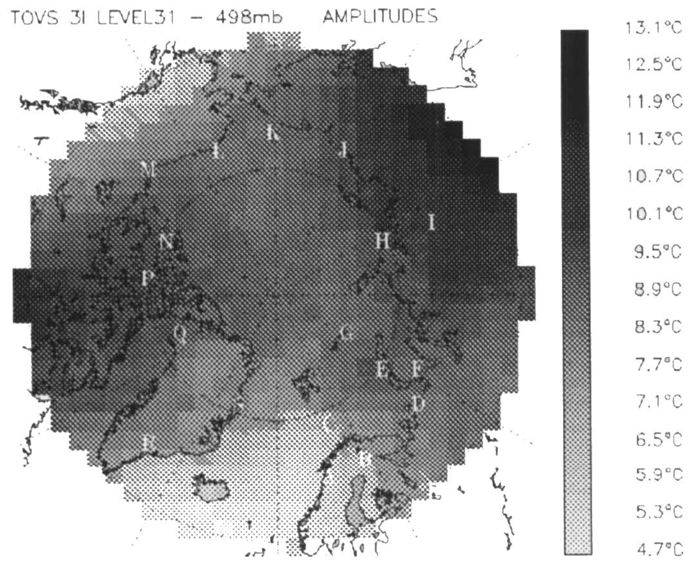

Fig. 5. Amplitude of the seasonal cycle in the TOVS 500 mbar retrieved temperatures over the Arctic Basin. Letters mark the locations of upper-air stations (see Fig. 7 for their amplitudes).

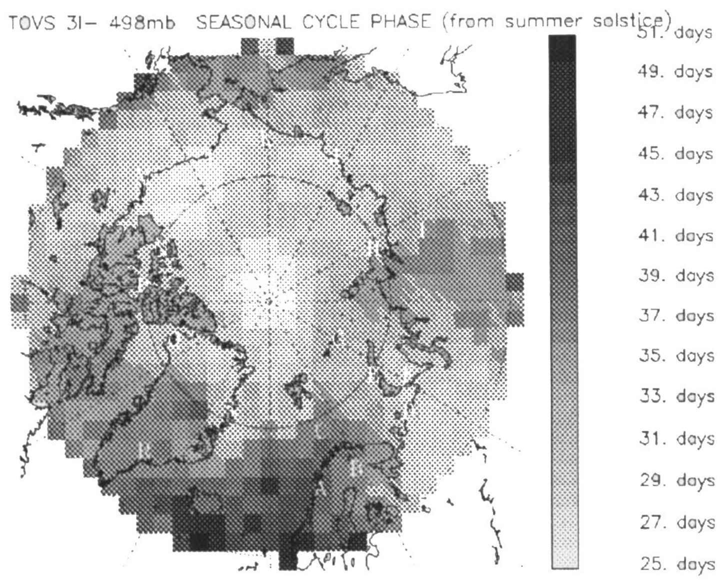

Fig. 6. Phase of the seasonal cycle (days since the summer solstice) in the TOVS 500 mbar retrieved temperatures over the Arctic Basin. Letters mark the locations of upper-air stations (see Fig. 7 for their phase values).

were observed. The six-hour difference in the times that these two satellites observe any given point on the globe was not expected to be important in the summer and winter seasons when there is little diurnal cycle. The biases observed were relatively constant, implying incorrect instrument correction factors. These factors were computed from radiosonde matchups from a global set. The authors suspect that these bias correction factors need to be recomputed for the Arctic, since the measurements have been made at the far end of the instruments' operating range (see Eyre 1987).

The sounding data were averaged onto an equal-area azimuthal polar grid, with grid cells 240 km on a side. This translated into 29 x 29 grid cells that encompass the area north of 60°N. Grid cells outside the 60°N parallel but within the outer bounds of the 29 x 29 square array were always treated as missing. Data at all sensor scan angles were included, since eliminating data at large scan angles leaves a data gap over the pole. However, data were weighted by the inverse of the scan angle. Thus, in data-rich regions, the less reliable data contributed little to the average. The mean of the weights for a given grid cell provided an indication of how much high-angle data were included in the average. Four parameters were computed and saved for each grid cell at each of 39 levels. These were: the weighted mean, the total number of soundings going into the average, the weighted standard deviation of the mean, and the mean weight of the soundings.

Ancillary data

The Historical Arctic Rawinsonde Archive (Kahl and others 1992) is a comprehensive collection of more than 1.2 million rawinsonde soundings. For most stations the record begins in 1958 and extends to 1987. Temperatures are interpolated to the first 24 pressure levels used in 3I, from the surface to 50 mbar.

The same analyses performed on the TOVS temperature retrievals were performed on the 500 mbar gridded data from the National Meteorological Center's (NMC) numerical forecast model. The NMC data were regridded from an octagonal grid onto the equal-area azimuthal grid that was used for the TOVS data. Twice-daily data were averaged into monthly means for the same period of record as the TOVS data.

Analyses and results

The analyses in this paper were based on monthly mean temperatures at 3I level 31, representing a layer from 472 to 525 mbar, for the period 1983–1991. This study was limited to a single level, although future work will examine other pressure levels in the data set. The analyses performed included a comparison of TOVS-derived and *in situ* profiles, a principal components analysis of spatial patterns, and an examination of trends in the principal component scores.

Retrievals

The strong, surface-based temperature inversions common to the Arctic present a major challenge to satellite temperature retrieval algorithms. Nonetheless, 3I was often successful in capturing surface inversions. The retrieved inversions were typically weaker than those found in the *in situ* data, but this was expected since the layer-averaged temperatures returned in the retrievals smooth out the strong gradients near the surface.

Figure 2 shows the difference between TOVS-derived profiles and rawinsonde data for mean January 1988 conditions at one Arctic station. At the level closest to the surface the retrieval is 3°C warmer than the station data, but the magnitude of the inversion is nearly 15°C. During summer, when low-level inversions are less intense, differences are typically much less.

A time series of monthly mean temperature anomalies for the TOVS/3I-derived and *in situ* 500 mbar temperatures at Narjan Mar is shown in Figure 3, starting in June 1983 and ending December 1991. While the overall agreement between the two was good ($r = 0.75$), there were clearly instances where the retrieved temperatures did not capture large deviations from one month to the next.

Seasonal cycle

The seasonal cycle of temperature T at each grid point was computed by first finding the mean for each month for all years, and then subtracting the mean for all months. The resulting 12 values were fit with:

$$T(m) = A \sin\left(\frac{2\pi m}{12} + \theta\right) \qquad [1]$$

where $m = 0.5, 1.5, ..., 11.5$. These fits return A as the amplitude and θ as the phase. A sample showing two cycles of the zero-mean monthly averages from Sodankyla along with the best fit sinusoid is given in Figure 4. In general, the amplitude was determined better than the phase, since the annual cycle was not always symmetric with respect to the seasons; for example, the summer warming may occur more rapidly than the winter cooling.

Figure 5 shows the amplitude of the seasonal cycle of temperatures at 500 mbar, and Figure 6 shows the phase. The peak-to-peak amplitude values were double what is shown. The amplitude was greatest over Siberia, with a peak-to-peak value of more than 25°C. A secondary maximum occurred over the Canadian archipelago, connecting with the primary maximum with a ridge over the pole. Minima occurred over the North Atlantic Ocean and Bering Sea. This pattern was in good general agreement with the amplitude of the NMC 500 mbar temperatures (not shown).

The phase of the temperature cycle is expressed as the number of days that the peak positive value occurs past summer solstice, June 21, or, equivalently, the number of days that the minimum occurs after the winter solstice, December 21. Figure 6 shows a maximum of about 50 days in the Greenland and Norwegian seas. This means that the maximum temperatures at the 500 mbar level occurred around August 10 in that area. The shortest phase occurred over the pole, about 25 days. This is probably determined more by the minimum occurring soon after the winter solstice. The phase is also short over the Beaufort Sea.

The seasonal cycle from selected upper-air stations was also computed and compared with TOVS values for the grid cells containing the stations. The stations are listed in Table 1 and the results are shown in Figure 7. The overall agreement between the amplitudes of the 3I retrievals and the upper-air stations was good ($r = 0.94$). One region of discrepancy between the TOVS and NMC seasonal cycles (not shown) was in the Beaufort Sea, where TOVS returned amplitudes of 16°C peak-to-peak and NMC has an amplitude of 18°C peak-to-peak.

The phase of seasonal cycle determined from NMC data was similar to TOVS in having a maximum lag over the Greenland and Norwegian seas. However, the maximum was roughly five days earlier. The minimum over the pole and Beaufort Sea was later by about 4–5 days. Also, there were other minima of the same size, around 30 days, over both Siberia and the Urals in the NMC data, which placed them within a few days' agreement with the TOVS data in these regions. Comparisons of TOVS and NMC phases with results from individual stations were mixed. For some stations, the match with TOVS was better, and for others the results were closer to the phases for NMC. Unfortunately, the region of greatest discrepancy between TOVS and NMC and of greatest interest, the Arctic Ocean, was also the region where there were little station data to resolve these discrepancies.

Table 1. Letter codes, WMO station numbers, and names of stations used for comparison of upper air data with TOVS soundings.

	WMO ID	*Station name*	*Latitude (° N)*	*Longitude (°E)*
A	1152	Bodo	67.28	14.42
B	2836	Sodankyla	67.37	26.65
C	1028	Bjørnøya	74.52	19.02
D	22271	Sojna	67.88	44.13
E	20744	Malye Karmakuly	72.38	52.73
F	23022	Amderma	69.77	61.68
G	20046	Gmo im et Krenkelya	80.62	58.05
H	21504	Ostrov Preobrazhenia	74.67	112.93
I	24125	Olenek	68.50	112.43
J	21965	Ostrov Chetyrekhstolbo	70.63	162.40
K	21982	Ostrov Vrangelya	70.97	181.47
L	70026	Barrow	71.30	203.22
M	71957	Inuvik	68.30	226.52
N	71072	Mould Bay	76.23	240.68
P	71924	Resolute Bay	74.72	265.05
Q	4202	Thule	76.53	291.25
R	4360	Angmagssalik	65.60	322.37
S	4339	Scoresby Sund	70.48	338.03

Spatial patterns of non-seasonal variability

One of the primary motivations of this work was the desire to know if there is significant variability in Arctic atmospheric temperatures that is not captured in the conventional rawinsonde record. The analysis of the seasonal cycle in the previous section suggested that this may be the case. To pursue this further, the spatial and temporal patterns of variability in the temperature anomalies — that is, the departures from the seasonal cycle — were examined. These departures were analyzed with principal components

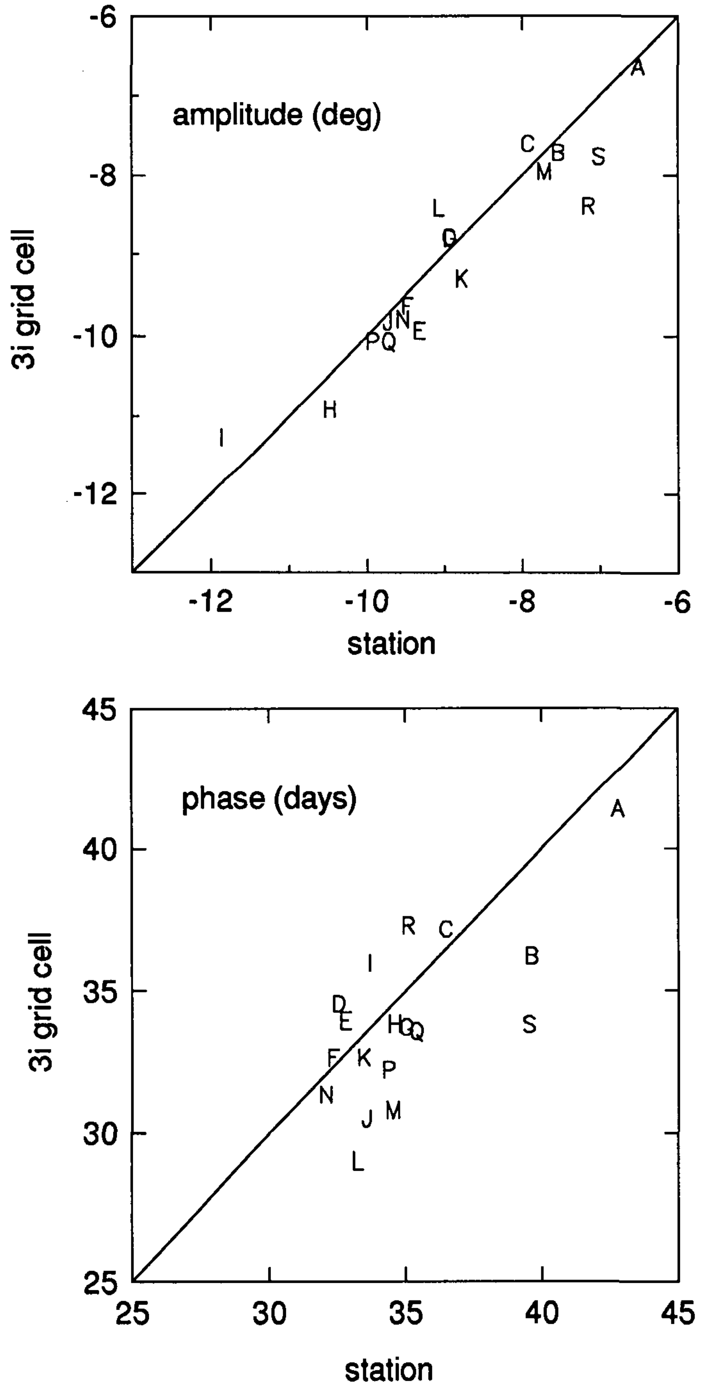

Fig. 7. Scatter plots of the seasonal cycles of 500 mbar temperature from TOVS-3I and station data: (a) amplitude; (b) phase.

analysis (PCA). Various types of factor analysis (PCA, empirical orthogonal functions (EOF), and singular value decomposition (SVD)) have been used extensively in the analysis of climatological data sets. Recently these methods have also been applied to remotely sensed data (compare Yulaeva and Wallace 1994).

In this study, principal components analysis sought to replace one set of variables with another set of statistically independent variables. These new variables were the principal components, or empirical orthogonal functions. The temperature at each grid location was a separate variable. The principal components were derived from the correlation between these variables over time, which would generally be high for neighboring cells and low for cells separated by large distances. The loadings, which could be positive or negative, defined the principal components, and were the correlations between the temperatures at each spatial location and the components. The loadings of each variable on each component therefore defined a new set of spatial patterns, summarizing the dominant patterns of correlation between spatial locations throughout the time period of the data set. While there are as many components as there are original variables, the first few typically accounted for most of the variance in the data. Principal component scores were the sum of the products of the loadings and the original, standardized variable values at a given time step. So, each grid of temperature was replaced by a set of principal component scores, which expressed the relative importance of the spatial pattern, represented by component loadings, as well as the temperature magnitude at that time step.

Several facts should be kept in mind when interpreting the results. First, the principal components of a given data set were orthogonal, but they were not unique; that is, a different set of principal components (PCs) may equally well have described the data. Thus, a one-to-one correspondence of the principal components in data from NMC and TOVS was very unlikely. Second, the patterns obtained would have been different if data from lower latitudes were included in the analysis. Third, only one atmospheric level was being examined. The patterns would probably be different at other levels.

Time series of anomalies were computed by subtracting from each monthly value the monthly mean for that grid cell, as computed through all years in the record. The first three principal components were then examined; the percent of the variance in the original data explained by each principal component is shown as a scree diagram in Figure 8. Components beyond the third explained less than 10% of the variance in the data and therefore were not considered further.

The strongest agreement between the TOVS and NMC data was in the second principal component (PC2) from each data set. Results are given in Figure 9, with positive and negative loadings shown separately. For the TOVS data this PC explained 12% of the variance. The dipole pattern shown in the loadings had one center over the Barents Sea and northern Ural mountains. Another, broader, center of opposite sign was spread out zonally from southern Greenland and across Canada. The time series of the scores of the second principal component for each data set correlated at $r = 0.73$, with excellent coincidence of the major extrema.

The third principal component of the TOVS data also

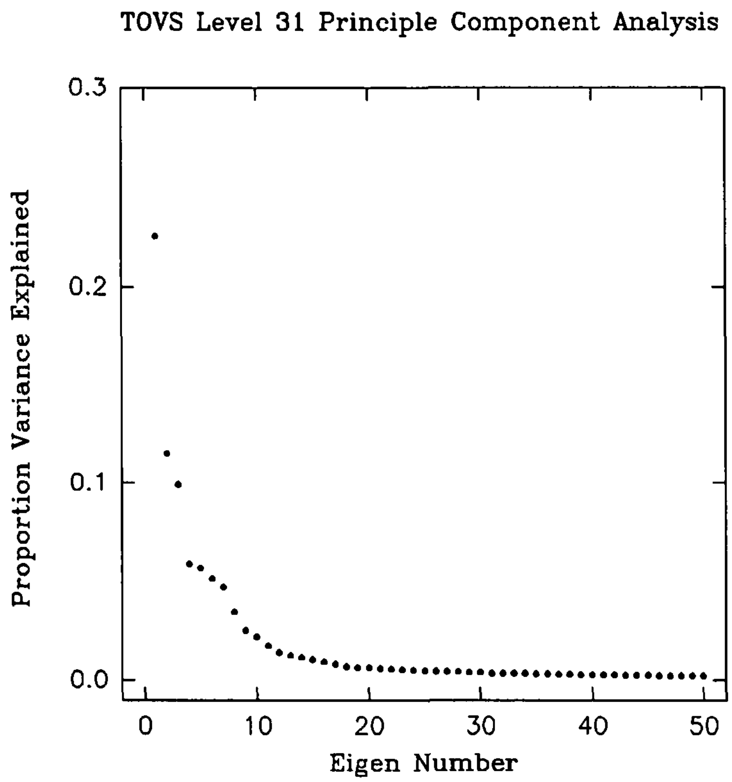

Fig. 8. Percent of the variance in the original temperature data explained by each principal component.

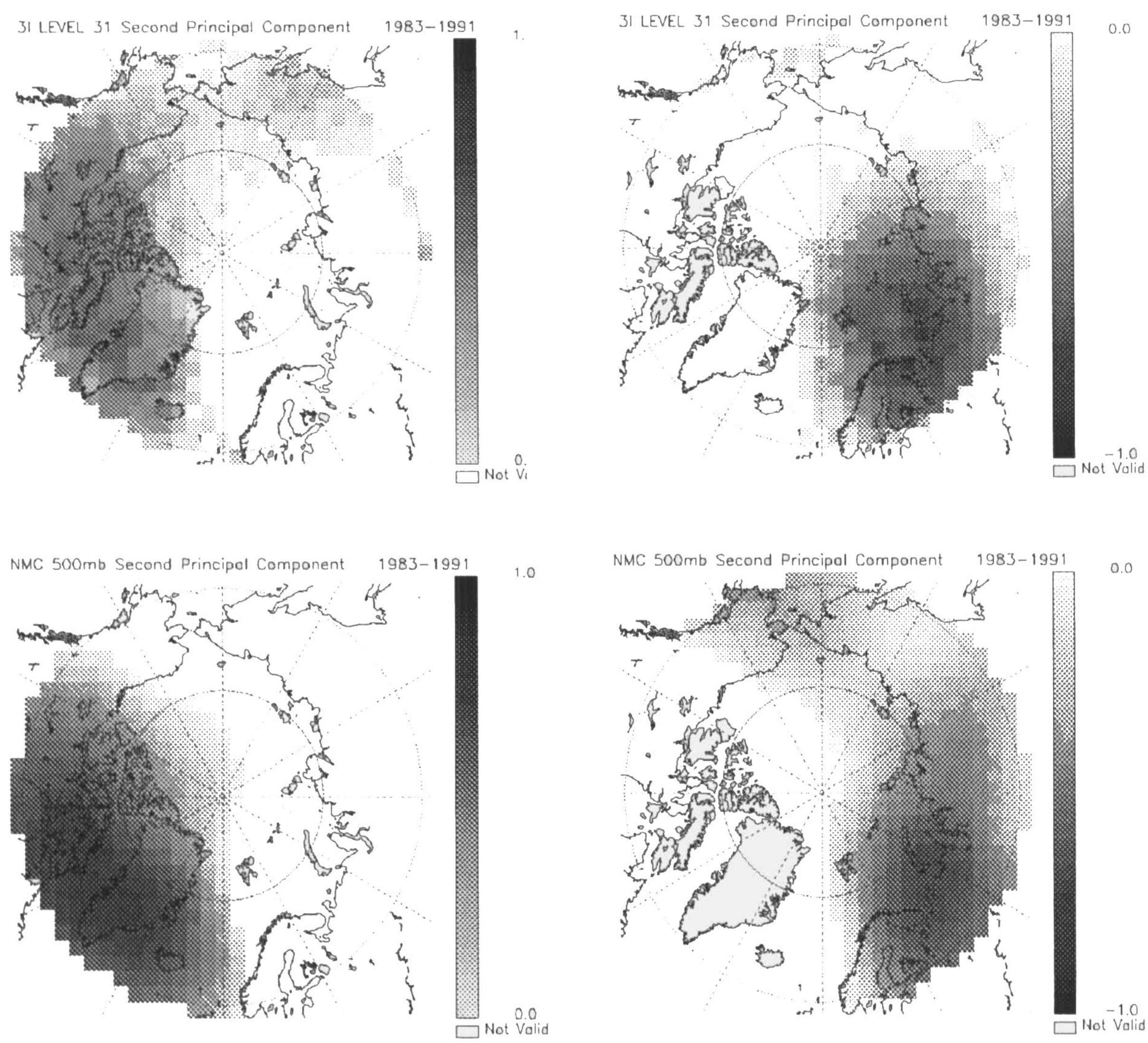

Fig. 9. Component loadings for the second principal components of the TOVS 500 mbar temperature (top) and the NMC analysis (bottom). Positive loadings are shown on the left; negative loadings are on the right.

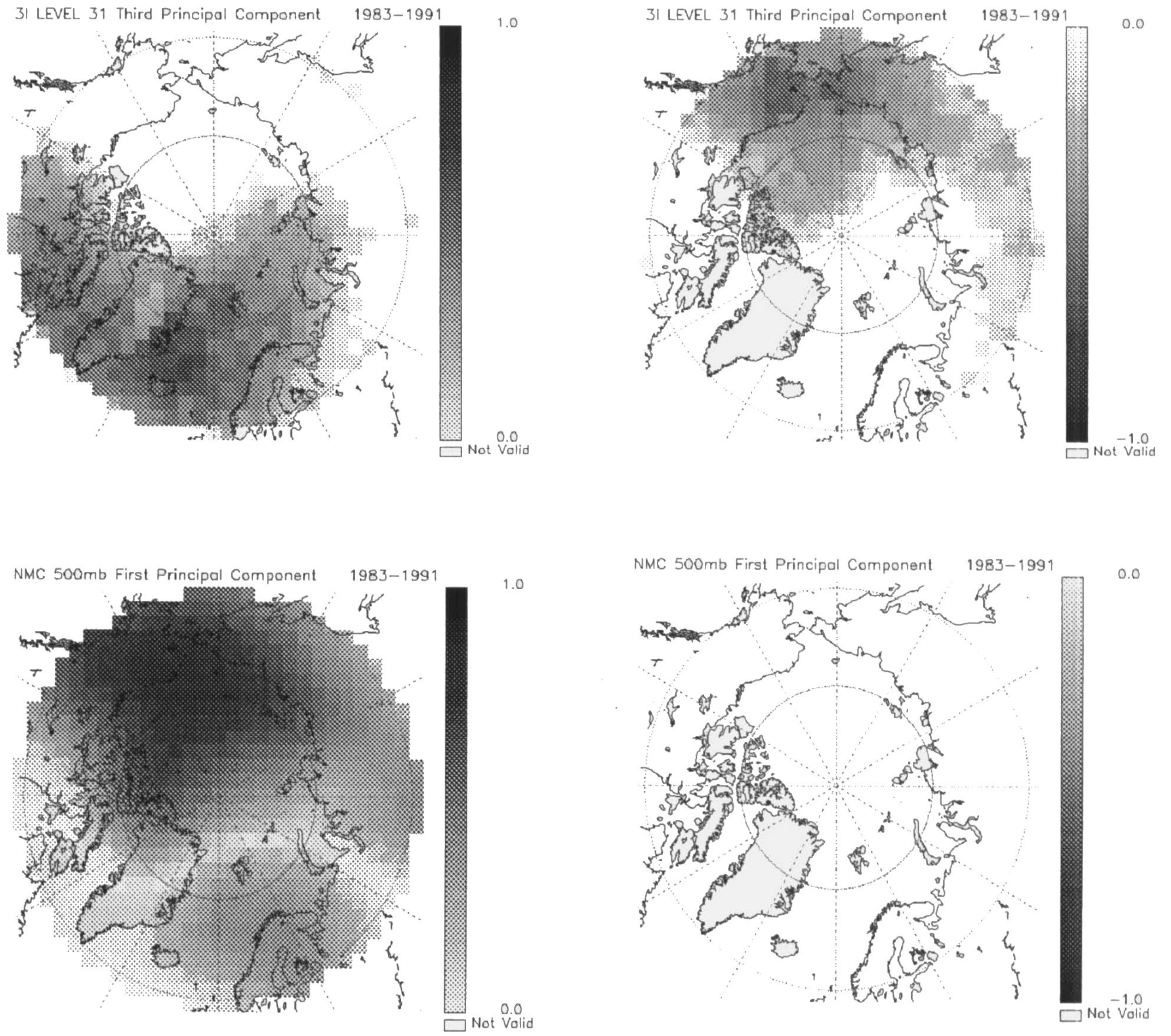

Fig. 10. Component loadings for the third principal component of the TOVS 500 mbar temperature (top) and the first principal component of the NMC analysis (bottom). Positive loadings are shown on the left; negative loadings are on the right.

had a dipole pattern (Fig. 10). It explained 10% of variance. One pole of this pattern was over Alaska and East Siberia, the other over the Greenland and Norwegian seas. Neither PC1 nor PC3 of the NMC 550 mbar data showed dipole patterns. Instead they were monopoles, roughly corresponding to each of the poles in TOVS PC3. The first principal component of the TOVS-3I temperatures and the third component of the NMC analysis are shown in Figure 11.

To verify that the dipole patterns seen in the second and third principal components of the TOVS data were actual modes of temperature variability in the Arctic atmosphere, rawinsonde data from a variety of high-latitude stations were correlated with the temperatures from the TOVS retrievals. The time series of departures from the seasonal cycle at each TOVS level 31 grid point were correlated with the departures for the 500 mbar level from the selected station. In Figure 12, the correlations with Scoresby Sund and with Barrow are shown. A maximum linear correlation, $r = 0.74$, occurred in the grid cell adjacent to the station location, shown by an 'X.' Positive correlations covered most of the North Atlantic Ocean, Greenland, and the region around Baffin Island. Negative values covered most of the Arctic Basin, Alaska, and all of northern Eurasia, with maxima up to $r = -0.44$ over northwestern Russia. This pattern was nearly identical to TOVS PC2 (Fig. 9). The correlations with Barrow showed that positive maxima of $r = 0.79$ were over Alaska, while negative values of up to $r = -0.44$ were spread over the Norwegian Sea. This reproduced the pattern seen in TOVS PC3 (Fig. 10).

Trend analysis in TOVS level 31 PC1

The time series of principal component scores for the first three components of the TOVS-3I 500 mbar temperatures are shown in Figure 13. The scores for PC1 show some of the major climatic events, such as the major coolings in the 1988/89 (Walsh and Chapman 1990) and 1990/91 winters.

Least squares linear fits were performed on the TOVS principal component scores. Only PC1 had a trend that

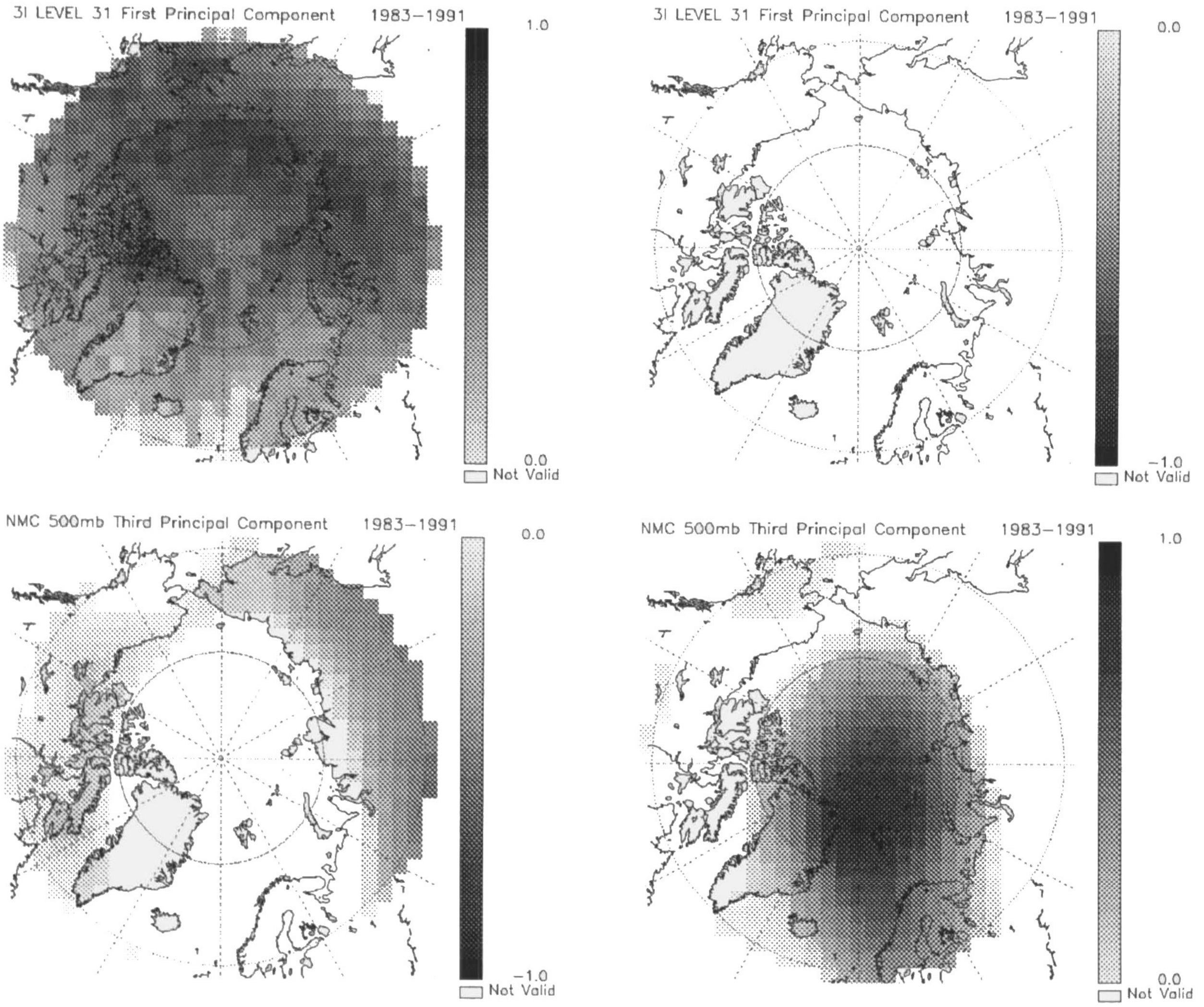

Fig. 11. Component loadings for the first principal component of the TOVS 500 mbar temperature (top) and the third NMC principal component (bottom). Positive loadings are shown on the left; negative loadings are on the right.

was significant above the 99% level. Since the loadings of PC1 were all of one sign, this implied a secular trend in the temperature departures. (A trend in the scores for a PC with a dipole pattern in the loadings could imply only that the pattern was strengthening or weakening.) The negative trend in PC1 indicated an interannual cooling over much of the Arctic, especially in the region of the Chukchi Sea and the East Siberian Sea. Data from Ostrov Chetyrekhstolbo and several stations in the region were examined. No significant trend was found in the time series from any of the stations. The correlations between 500 mbar temperatures from these stations and the TOVS level 31 data at the location of peak loading for PC1 were significant, but arose mainly from extreme events, not a similarity in trends. None of the scores from first three PCs of the NMC data had significant trends.

Kahl and others (1993b) examined the historical Arctic rawinsonde record for evidence of greenhouse warming over the period 1958–1986. The temperature trends they found mostly fell below a 90% significance level. Those that did exceed this significance level were mixed with respect to sign and varied by season. Significant negative trends during the northern autumn and winter were observed for the 500–400 mbar layer in the far northern Canadian archipelago and the coasts of Greenland. While these results were in partial agreement with the trends seen in TOVS PC1, Kahl and others' analysis was limited to coastal stations. In another study, Kahl and others (1993a) examined data from drifting Soviet ice islands and dropsondes released from weather reconnaissance aircraft. These data covered the western and central Arctic Ocean. For the period 1950–1990 it was found that significant cooling in surface air temperatures was accompanied by a warming in the 700–850 mbar layer. These results did not compare readily with the current study since in the analysis of Kahl and others (1993a) the data were not from a fixed location and little could be said about the spatial distribution of temperature trends.

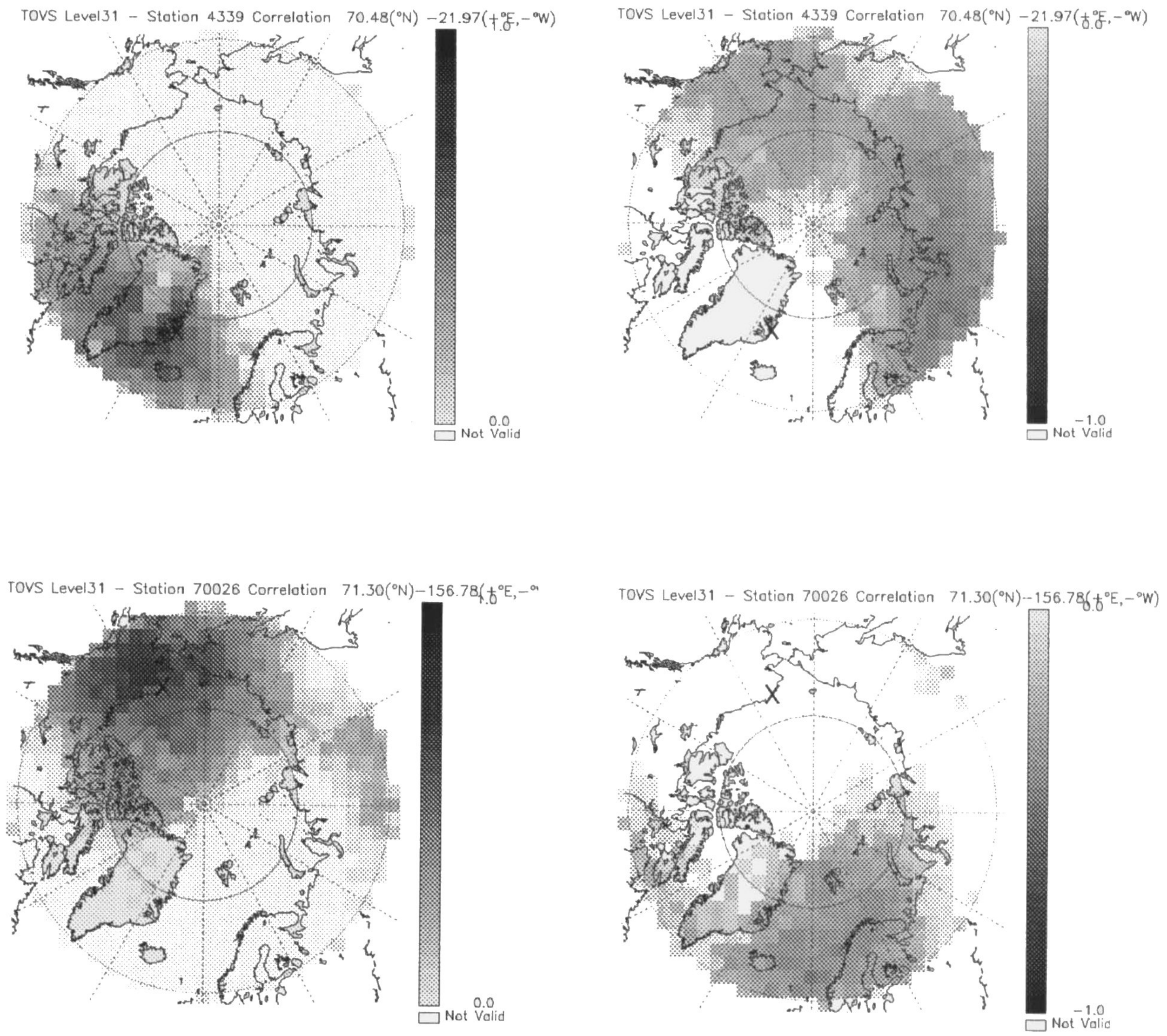

Fig. 12. Linear correlations between the TOVS 500 mbar temperatures and those from two upper-air stations: (a) Scoresby Sund (#4339) at 70°N, 22°W, and (b) Barrow (#70026) at 71°N, 157°W.

Summary and conclusions

The Earth's high-latitude regions are of critical importance in many scenarios of climate change, but a time-continuous, spatially complete, and well-calibrated record of tropospheric temperatures is needed in order to assess past and future climate changes. Analysis of a portion of the 16-year data record of the TIROS Operational Vertical Sounder (TOVS) aboard NOAA polar-orbiting satellites has allowed an examination of both the spatial and temporal variability of mid-tropospheric temperatures in the Arctic. Although the period of the TOVS record is relatively short for climate studies, it is adequate for identifying the principal modes of Arctic temperature variability. This helps determine whether the longer but spatially inhomogeneous rawinsonde record captures all significant features of this variability. This study also provides a baseline against which future climate variability in the Arctic can be assessed.

Temperature retrievals based on clear-column radiances archived at NOAA/NESDIS were done using algorithms tuned to the Arctic. Retrievals of the temperature profile using the 3I (Improved Initialization Inversion) method with NOAA/NESDIS clear-column radiances were first compared to historical Arctic rawinsonde data for selected cases. In general, retrievals were good, although strong, low-level inversions were problematic. Time series of 500 mbar temperatures in the TOVS, NMC, and rawinsonde data were examined and the seasonal cycles were described in terms of amplitude and phase. The spatial distribution of amplitudes determined for the various data sets agreed well but there was less agreement in the phase comparisons. One of the areas of greatest discrepancy between NMC and TOVS was over the pole, where there are little *in situ* data to assist in resolving the differences.

Principal component analysis was used to examine spatial patterns in the temperature departures (seasonal means removed) for TOVS and NMC data. Both monopole and dipole patterns were observed in the component loadings, one pair of patterns being nearly identical between the two data sets. Spatial patterns of the correlation

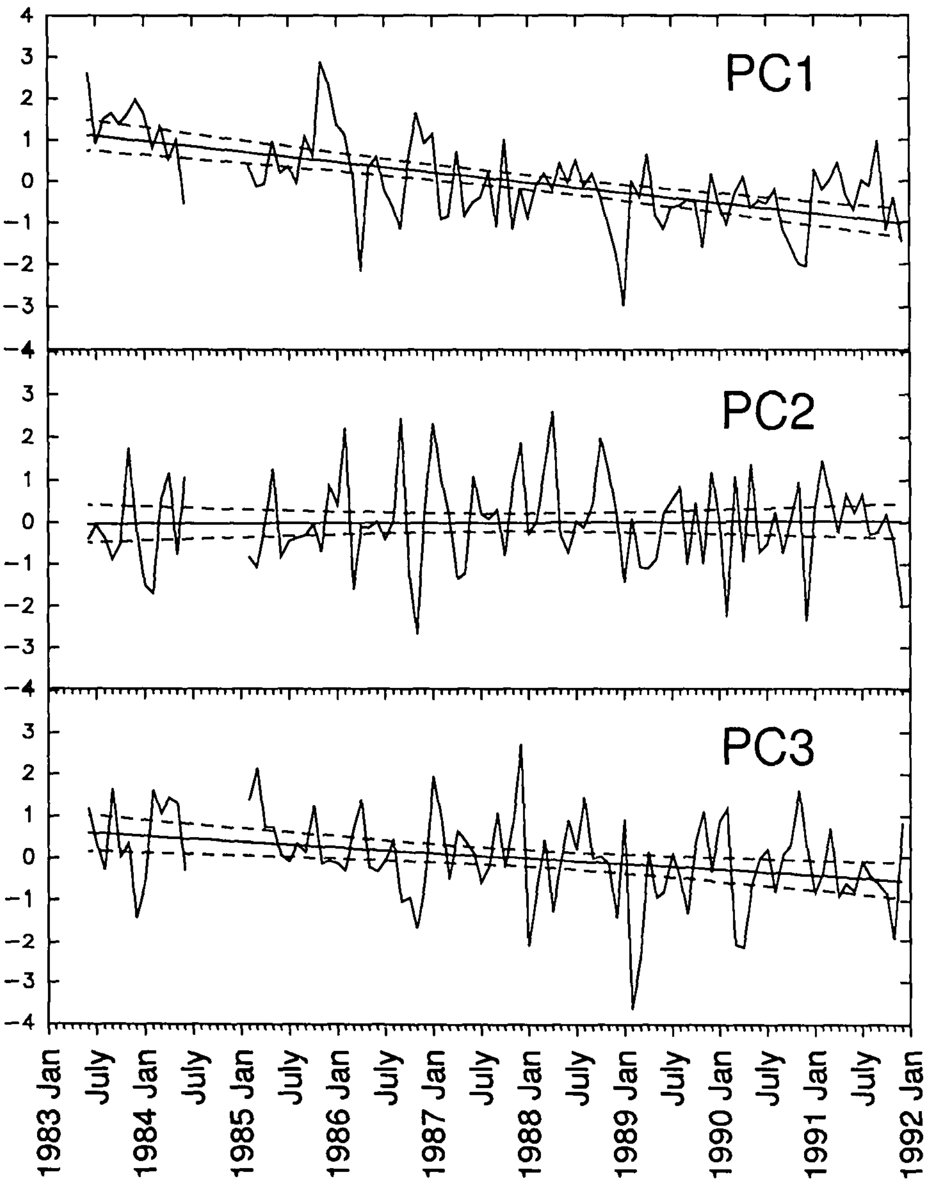

Fig. 13. Times series of principal component scores for the TOVS 500 mbar analysis (principal components 3l level 31). Also shown are the linear regression fits to the series (solid line) and the 95% confidence interval.

between the upper-air data and the TOVS retrievals revealed patterns similar to the principal component loadings. Finally, the time series of component scores were analyzed for trends. No significant trend was found in the station data but a significant negative trend was found in the first principal component scores of the TOVS retrievals.

The Arctic temperature data set derived from TOVS provides an important adjunct to data currently available from other sources. The land-based upper-air network does not provide coverage of the Arctic Ocean, which the analysis shows has significant features in the spatial patterns of temperature variability. Data from the drifting ice island and dropsonde programs do not have the spatial or temporal continuity needed to study patterns of variability in any detail. Data from NMC are spatially complete and continuous, but incorporate little, if any, data from the central Arctic Ocean in the model analysis. Agreement between NMC and TOVS results is good in some cases, but TOVS appears to provide more detail and perhaps greater accuracy. Future work will explore further the utility of this data set by examining other levels of the atmosphere.

Acknowledgements

This study was supported by NOAA grant no NA26GP0186 and NASA grant no NAGW-2407. Thanks are due to G. Mandler and H. Maybee, who performed most of the programming and graphics work .

References

Chedin, A., N.A. Scott, C. Wahiche, and P. Moulinier. 1985. The improved initialization inversion method for temperature retrievals from satellites of the TIROS-N series. *Journal of Climate and Applied Meteorology* 24: 128–143.

Eyre, J.R. 1987. On systematic errors in satellite sounding products and their climatological mean values. *Quarterly Journal of the Royal Meteorological Society* 113: 279–292.

Francis, J.A. 1994. Improvements to TOVS retrievals over sea ice and applications to estimating Arctic energy fluxes. *Journal of Geophysical Research* 99 (D5): 10,395–10,408.

Hansen, J., and Lebedeff, S. 1987. Global trends of measured surface air temperature. *Journal of Geophysical Research* 92: 13,345–13,372.

Kahl, J.D., D.J. Charlevoix, N.A. Zaitseva, R.C. Schnell, and M.C. Serreze. 1993a. Absence of evidence for greenhouse warming over the Arctic Ocean in the past 40 years. *Nature* 361: 335–337.

Kahl, J.D., M.C. Serreze, S. Shiotani, S.M. Skony, and R.C. Schnell. 1992. In situ meteorological sounding archives for Arctic studies. *Bulletin of the American Meteorological Society* 73 (11): 1824–1830.

Kahl, J.D., M.C. Serreze, R.S. Stone, S. Shiotani, M. Kisley, and R.C. Schnell. 1993b. Tropospheric temperature trends in the Arctic: 1958–1986. *Journal of Geophysical Research* 98 (D7): 12,825–12,838.

Key, J., S.J.S. Khalsa, and J. Bates. 1993. Assessing the completeness of the TIGR data base for Arctic retrievals. In: Menzel, W.P. (editor). *Seventh International TOVS Study Conference (ITSC-VII), Igls, Austria, 10–16 February.* Madison, WI: University of Wisconsin: 200–208.

Manabe, S., M.J. Spelman, and R.J. Stouffer. 1992. Transient responses of a coupled ocean–atmosphere model to gradual changes of atmospheric CO_2. Part II: seasonal response. *Journal of Climate* 5: 105–126.

McMillin, L.M., and A. Nappi. 1986. Some modifications to the NESDIS operational clear column radiance procedure. In: Eyre, J.R. (editor). *Technical proceedings of the Third International TOVS Study Conference.* Reading: European Centre for Medium-range Weather Forecasts: 160–172.

Serreze, M.C., J.D. Kahl, and R.C. Schnell. 1992. Low-level temperature inversions of the Eurasian Arctic and comparisons with Soviet drifting station data. *Journal of Climate* 5 (6): 615–629.

Walsh, J.E., and W.L. Chapman. 1990. Short-term climatic variability of the Arctic. *Journal of Climate* 3: 237–250.

Wetherald, R.T., and S. Manabe. 1988. Cloud feedback processes in a general circulation model. *Journal of Atmospheric Science* 45: 1397–1415.

Yulaeva, E., and J.M. Wallace. 1994. The signature of ENSO in global temperature and precipitation fields derived from the microwave sounding unit. *Journal of Climate* 7: 1719–1736.

The accuracy of references in the text and in this list is the responsibility of the authors, to whom queries should be addressed.